MICROCOPY RESOLUTION TEST CHART
NATIONAL BUREAU OF...

COMPARISON OF NUMERICAL RESULTS AND MEASURED DATA FOR
SMOOTH AND INDENTED NOSETIPS

Tsuying Hsieh
Naval Surface Weapons Center, White Oak, Maryland

ABSTRACT *14 May 81*

Numerical calculations, using an unsteady implicit numerical algorithm which solves either the inviscid or the thin-layer Navier-Stokes equations, were performed for smooth and severely indented nosetips at hypersonic speed and zero angle of attack. The computed results of inviscid and laminar flowfield are compared to wind tunnel measured data for surface pressure, shock location, heat transfer and density distribution in the shock layer. Good agreements between the calculated and measured flowfield are obtained for smooth nosetip without flow separation. Difficulties in the simulation of severely indented nosetips with large separation bubble or sharp corner are discussed.

NOMENCLATURE

C_p = Pressure coefficient, $p-p_\infty/\frac{1}{2}\,\rho_\infty\,U_\infty^2$

J,K = Index of grid in the streamwise and body-to-shock direction respectively

L = Reference length, 2.56 cm (1 in.)

M = Mach number

n = normal direction

p = pressure

Pr = Prandtl number

R = Radius of circular arc

Re = Unit Reynolds number, U_∞/ν

Rs = Radius of sphere

S = Arc length

St = Stanton number $= \dfrac{(\mu_\ell + \mu_t)/\mu_\infty}{Re_\infty\,(Pr_\ell + Pr_t)}\left[\dfrac{T_o}{T_\infty} - \dfrac{T_w}{T_\infty}\right]^{-1}\dfrac{\partial(T/T_\infty)}{\partial(n/L)}$

t = time

T = temperature

II-297

82 03 09 11

U = Velocity

X,Y = Axial and radial coordinates respectively

ρ = Density

εE = Coefficient for explicit dissipation

εI = Coefficient for implicit dissipation

ν = Kinematic viscosity of fluid

<u>Subscript</u>

∞ = free stream

ℓ = laminar flow

o = stagnation point

t = turbulent flow

w = wall

INTRODUCTION

Because of ablation, the nosetip of a spherical body undergoes continuous change during re-entry. The shape of the nosetip has a great influence on the flowfield over the entire body, i.e., the nose region and thus the afterbody. In order to understand the flowfield about indented nosetip shapes that are likely to occur during the re-entry process, considerable effort has been expended both experimentally and theoretically.[1-4] (also see references listed in Ref. 1 and 2).

Among the experimental work, Refs. 3 and 4 provide a comprehensive set of measurements for a systematic change of nosetip shapes. This includes surface pressures, heating rates, flowfield pictures using electro-optical techniques and velocity mapping using Laser Doppler Velocimeter. These experiments are intended to provide basic information about the important flow features to be expected in the flowfield and also serve as a useful data base for the development of a numerical code to predict the flowfield.

Among the many numerical schemes intended for indented nosetip calculation, a promising and versatile one seems to be due to Kutler et al.[1] As described in Ref. 1, Kutler et al solved the unsteady Navier-Stokes equations with the "thin-layer" approximation for nosetip of arbitrary shapes at zero indicence using the implicit factored numerical algorithm of Warming and Beam.[5] The steady solution is obtained asymptotically in time and both viscous and inviscid flowfields can be computed using the same computer program, refered to as K-C-L code in this paper. As described in Ref. 2, when the inviscid portion of the K-C-L code was applied to the nosetip shapes reported in Ref. 3 and 4 surmountable difficulties were encountered during the course of calculation because of the presence of small radius expansion corners and a

concave compression turn in these nosetips. It was later found that a special
calculation procedure is required in order to obtain reasonable solutions.

For the details of the numerical procedure used in the K-C-L code and the
special calculation procedure for the indented nosetip computation, the
readers should consult to Ref. 1 and 2 and will not be repeated in this paper.
The same calculation procedure has since been applied to compute viscous flow
over smooth and indented nosetips and several typical results will be described
and compared to measured data.

II. RESULTS AND DISCUSSION

A. Smooth Nosetips

The comparison of inviscid results for surface pressure and density
distribution over a sphere is reproduced here from Ref. 2 as shown in Fig. 1.
The grid used in the computation is J = 32 (along body surface) x K = 12
(across the shock layer) and the total number of time steps used is 600
(with a courant number of 2.5). This requires about 2 minutes CPU time in
CDC-7600 computer. The surface pressure is compared to the work of Inouye
and Lomax[6] and the measured data of Baer[7] as shown in Fig. 1a. The density
distribution in the shock layer is compared to the measured data of
Sedney and Kahl[8] as shown in Fig. 1b. The agreement are seen to be very good.

Viscous flow calculations based on the thin-layer approximation of Navier-Stokes
equations, were performed for a hemisphere-cone under the following flow
condition: $M_\infty = 5.92$, $Re_\infty = 5.5 \times 10^6$/ft and $Tw/T_\infty = 4.78$. A grid of 28x32
was used. For laminar calculation, 400 time steps with a Courant number (CN)
of 75 can be considered as the final solution (the nondimensional shock speed
is in the order of 10^{-3} and the CPU time is about 5 min). As shown in Fig. 2
the calculated results for heat transfer in term of Stanton number over the
surface is compared to the measured data reported in Ref. 7. Also plotted
in Fig. 2 is the boundary layer calculation using Cebeci-Smith's boundary
layer code as given in Ref. 7. It is seen that the agreement is satisfactory.
It should be noted that for hemisphere-cone, the flow is fully attached. The
surface pressure agrees well among the inviscid and laminar calculation as
well as the measured data. Therefore, the good agreement in heat transfer
between the boundary layer and the thin layer N-S calculation is to be expected.

In the numerical procedure, there are two kinds of dissipation used for
stability purpose, i.e., the explicit and implicit dissipation terms with
coefficients of ε_E and ε_I respectively. For inviscid and laminar calculation,
solution can be obtained without the implicit dissipation. For turbulent calculation,
it was found that the implicit dissipation must be added in order to have a
converged solution. Since the implicit dissipation terms have no effect on the
solution as the steady state is approached, it is therefore used in both laminar and
turbulent calculation. The explicit dissipation terms, on the other hand,
will always present. In viscous flow calculation, it is desirable that the
explicit dissipation coefficient be kept minimum so that the real viscous
effects can be simulated. From the experience for indented nosetip calculation,
the value of ε_E cannot be too small in order to have a smooth bow shock (no
wiggling) where the flow can essentially be assumed to be inviscid. Therefore,
the ε_E value in the η direction is linearly reduced to one tenth of the input

value toward the wall in order to minimize its effects there. This devise also consistent with the thin-layer approximation. When εE is linearly reduced, it is denoted by $\varepsilon E'$ to distinguish from the uniform one. As shown in Fig. 2, the effects of $\varepsilon E'$ are seen to be insignificant in the heat transfer results for hemisphere-cone with $\varepsilon E'$ varies from 0.1 to 0.02 and $\varepsilon I = 3 \varepsilon E'$. This is not so for indented nosetip calculation.

In the simulation of turbulent flow, the turbulence model of Baldwin and Lomax[9] was used. The final laminar solution with $\varepsilon E = 0.1$ was used as the initial flowfield for turbulent calculation. A turbulent solution was produced in 200 time steps with the nondimensional shock speed in the order of 10^{-3}. As shown in Fig. 2, the Stanton number increase significantly for turbulent flow as compared to the laminar flow one (no measured data for comparison). It should be pointed out that the surface pressure obtained from the laminar and turbulent solution agree to two digits.

B. Indented Nosetips

The special calculation procedure for inviscid flow over indented nosetips as described in Ref. 2 was applied to calculate viscous flow over indented nosetips. Model 1 and 4 as described in Ref. 2 were chosen for this investigation. The simulation of viscous turbulent flow over indented nosetips has not been very successful as described in the following paragraphs.

Laminar flow over Model 4 was first calculated. The calculation started with a grid of 24 x 32 (CN = 150, $\varepsilon E = 0.4$, $\varepsilon I = 0$) for 400 time steps to obtain a laminar solution over a sphere at $M_\infty = 5.0$, Re = 8 x 10^6/FT and $Tw/T_\infty = 5.4$. The sphere was then deformed to the shape of Model 4 in 1800 time steps. The grid was then increased to: (!) 58 x 32 and (B) 56 x 48 in another 1600 time steps each with the final values of CN = 50, $\varepsilon E = 0.1$ for (A) and $\varepsilon E' = 0.3$ for (B). The calculated surface pressure and shock locations from these two solutions are close (results not shown). This provides a self verification of the results. Since grid (B) contains more points in the η direction, its solution resolves the flow field better and is used for comparison as shown in Fig. 3 and 4.

Unlike the hemisphere-cone, the turbulent calculations for Model 4 encountered serious difficulties. Large amplitude oscillation of pressure in the flowfield quickly interrupted the computation. The value of CN was gradually reduced and the value of εI was increased ($\varepsilon E' = 0.3$ was maintained). At CN = 2 and $\varepsilon I = 6$, it was possible to run for 200 time steps with the non-dimensional shock speed coverging to a value of 0.04. The shock speed is then started to increase slowly but steadily. A further increase of εI up to 12 would not help to obtain a converged solution. Thus, the solution before the shock speed started to increase is shown in Fig. 3 and 4 for comparison. It is understood that the turbulent solution shown in Fig. 3 and 4 is not the converged solution.

Fig. 3 shows the comparison of shock location between calculations and experiments. The inviscid shock layer is thinner around the indented region as expected. The laminar and turbulent solutions for shock location are almost coincide and fall in between the inviscid solution and the measured data. The primary separation bubble indicated by the laminar solution is

smaller than observed experimentally. The laminar separation point of the
primary separation bubble is at the downstream end of the expansion corner,
but the flow picture (Fig. 8a of Ref. 2) shows that the flow separates
immediately at the beginning of the expansion corner. In general, the
effects of turbulence is to move the separation point toward downstream and
the separation bubble will be smaller. This fact suggests that the discrepancy
is not because of turbulence effects but from some other sources which are not
captured in the numerical solution. Also the laminar solution indicates that
there is a secondary separation bubble within the primary separation bubble
as sketched in Fig. 3. The secondary separation bubble was not reported
in Ref. 4.

In Fig. 4, the surface pressure distribution obtained from the inviscid,
laminar and turbulent solution are compared to the measured data. It is
noted that the viscous solutions compare better with the measured data than
the inviscid curve. The region around the expansion corner S/L $\sim$ 0.26 - 0.7
where the inviscid and viscous solutions are seen to agree well (i.e., no
flow separation) but are lower than the measured data. The dip in the
pressure curve in the region S/L $\sim$ 2.5 (where the secondary separation
bubble starts) is not shown by the measured data. A calculation was made with
the complete Navier-Stokes equation for laminar flow with the same grid
distribution as used in the thin-layer approximation calculation and the
results for surface pressure agree up to two digits.

For Model 1, there is a sharp expansion corner with a radius of 0.062 inch.
Three grid points were used to cover the corner as was done for the inviscid
calculation reported in Ref. 2 and a total grid points of 33x32 were used for the
viscous calculation. Only laminar solution can be obtained. As shown in Fig 5
and 6, the inviscid solution agrees reasonably well with the measured data for
both the shock location and the surface pressure because the separation bubble
is small as indicated by the flow picture (Fig. 5a of Ref. 2). In contrast to
the result of Model 4, however, the laminar solution indicates that the flow
separates immediately after the corner and form a large primary separation bubble
as shown in Fig. 5. Within the primary separation bubble, there is also a
secondary separation bubble around the location of compression turn. As a result
of the primary separation bubble, the laminar shock layer becomes thicker near the
separation bubble and thinner afterwards as compared to the measured data. Also the
surface pressure obtained from the laminar solution looks entirely wrong.

It was not possible to obtain a turbulent solution for Model 1, not even
one like that of Model 4. The obvious reason is that the laminar solution is
too far off from the measured data, which is assumed to be close to the turbulent
solution, therefore the starting flowfield is too poor to carry through the
calculation.

II-301
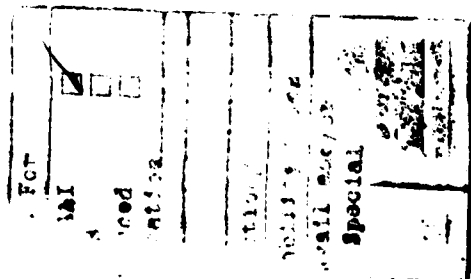
From the above comparison of results, it is concluded that the numerical code works well for smooth nosetips. For those indented nosetips investigated in this paper, the code fail to give a satisfactory solution. Possible reasons for the failure of the code to obtain a solution and for the discrepancy between the viscous calculation and the experimental data are suggested as follows: (1) The turbulence model used is inadequate. (2) The first-order-accurate numerical procedure is not sufficient to simulate the complicated flowfield. (3) The grid points and their distribution are insufficient to resolve the viscous effects. (4) The sharp corner as described in Model 1 requires special treatment to avoid flow separation introduced from sources other than the viscous effects. (5) Because of the prevailing of a large separation bubble, the thin-layer approximation may lead to wrong solution, i.e., for a significant portion of the flowfield, the viscous terms in both the ξ and η directions should be kept.

REFERENCES

1. Kutler, P., Chakravarthy, S. R. and C. P. Lombard "Supersonic Flow Over Ablated Nosetips Using an Unsteady Implicit Numerical Procedure" AIAA Paper 78-213, Jan 16-18, 1978.

2. Hsieh, T., "Numerical Investigation of Flowfield About a Series of Indented Nosetips," AIAA Paper No. 81-0077, Jan. 1981.

3. Ragsdale, W. C. and Morrison, A. M., "IAP 202 Heat Transfer and Pressure Tests in the NSWC/WOL Hypersonic Tunnel," NSWC/WOL MP 78-18, October 27, 1978.

4. Yanta, W. J., "Indented Nose Flowfield Tests," WTR 1329, Naval Surface Weapons Center, White Oak, MD., July 1980.

5. Warming, K. F. and Beam, R., "On the Construction and Application of Implicit Factored Schemes for Conservation Laws," SIAM, ATNS Proceedings, Vol. 11, 1978, pp. 85-129.

6. Inouye, M. and Lomax, H., "Comparison of Experimental and Numerical Results for the Flow of a Perfect Gas About Blunt-Nosed Bodies," NASA TN D-1426, Sept 1962.

7. Baer, A. L., "Pressure Distribution on a Hemisphere Cylinder at Supersonic and Hypersonic Mach Numbers," AEDC TN-61-96, Arnold Engineering Development Center, 1961.

8. Sedney, R. and Kahl, G. D., "Interferometric Study of the Blunt Body Problem," Ballistic Research Laboratory Report No. 1100, 1960.

9. Baldwin, B. S. and Lomax, H. "Thin Layer Approximation and Algebraic Model for Separated Turbulent Flow" AIAA Paper 78-257, 1978.
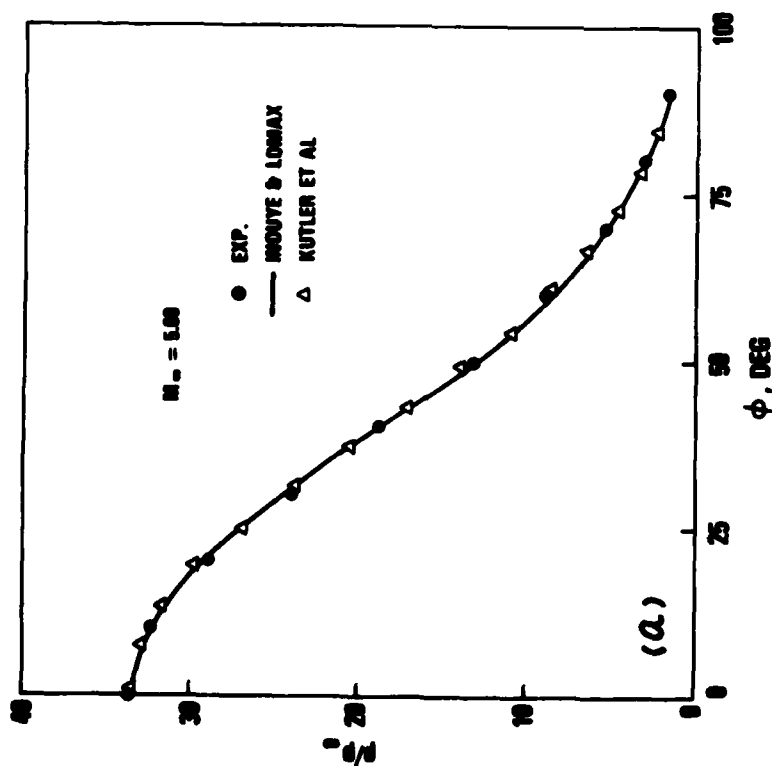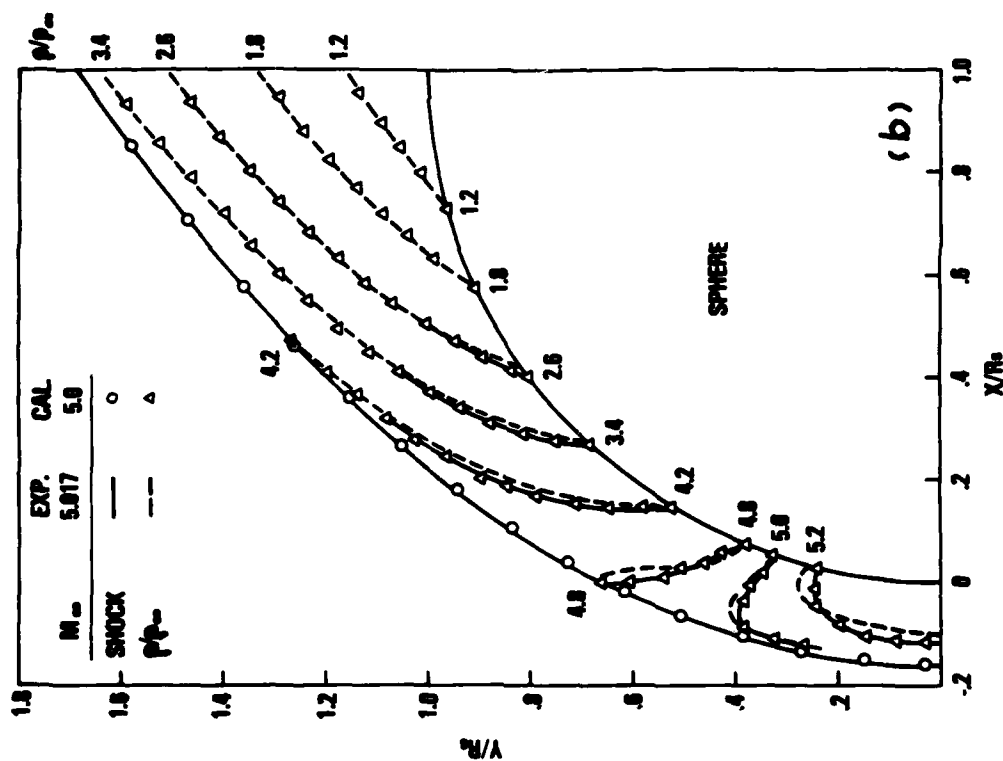
Figure 1   Comparison of Surface Pressure and Density Field
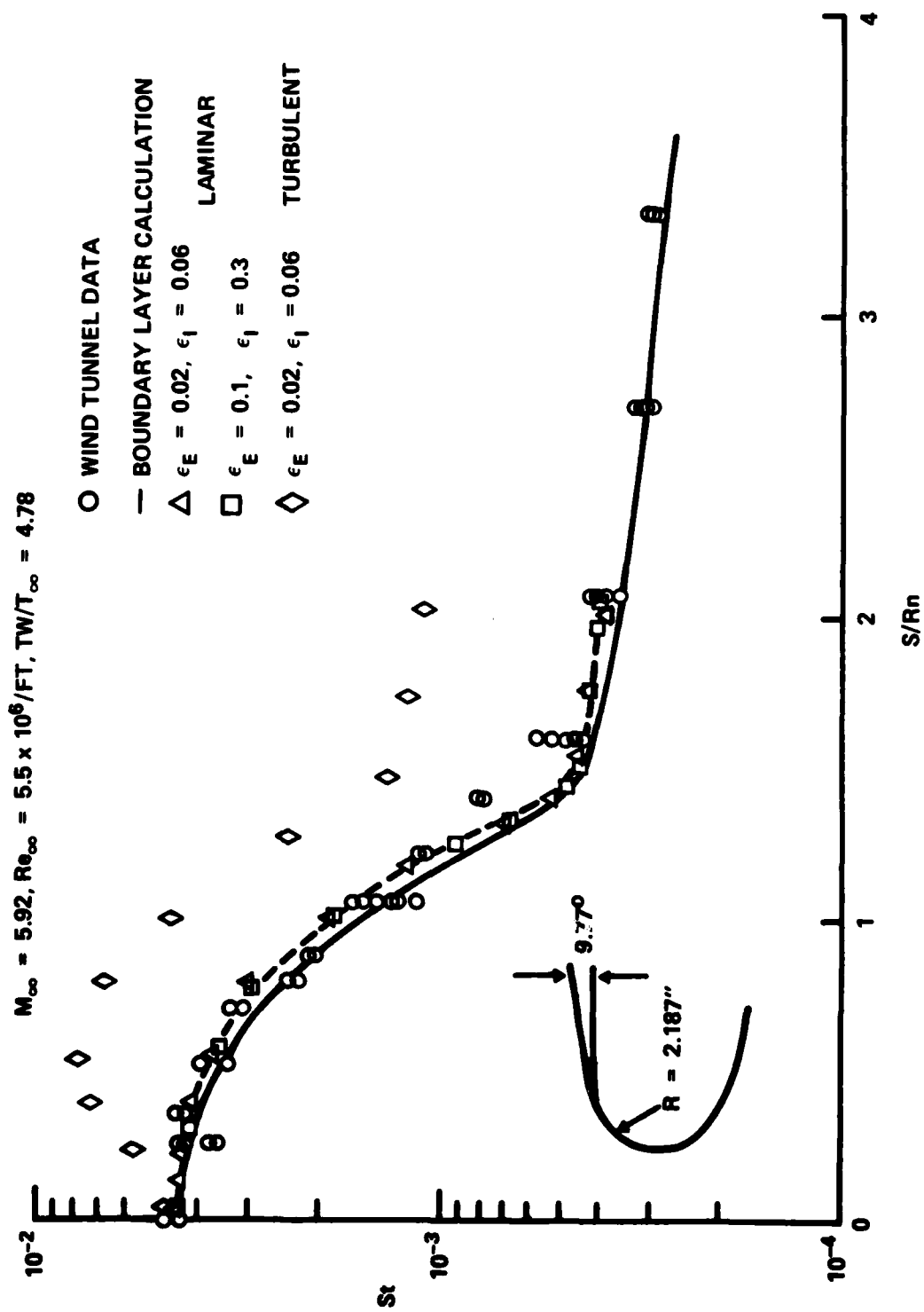Between Calculation and Experiment

$M_\infty = 5.92$, $Re_\infty = 5.5 \times 10^6/FT$, $TW/T_\infty = 4.78$

○ WIND TUNNEL DATA

— BOUNDARY LAYER CALCULATION

△ $\epsilon_E = 0.02$, $\epsilon_I = 0.06$ LAMINAR

□ $\epsilon_E = 0.1$, $\epsilon_I = 0.3$

◇ $\epsilon_E = 0.02$, $\epsilon_I = 0.06$ TURBULENT

FIGURE 2 COMPARISON OF HEAT TRANSFER MEASUREMENTS ON A HEMISPHERE CONE
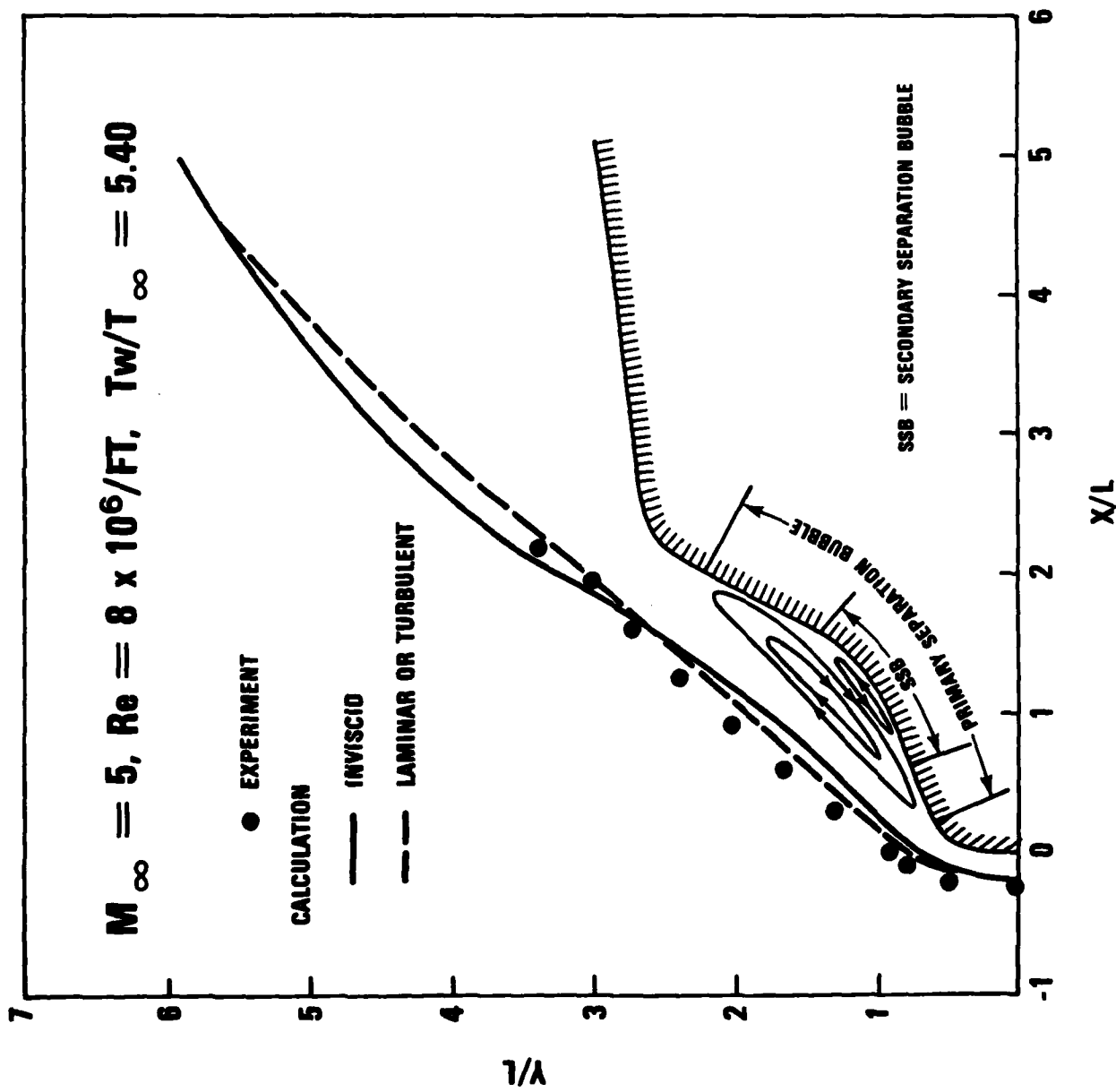
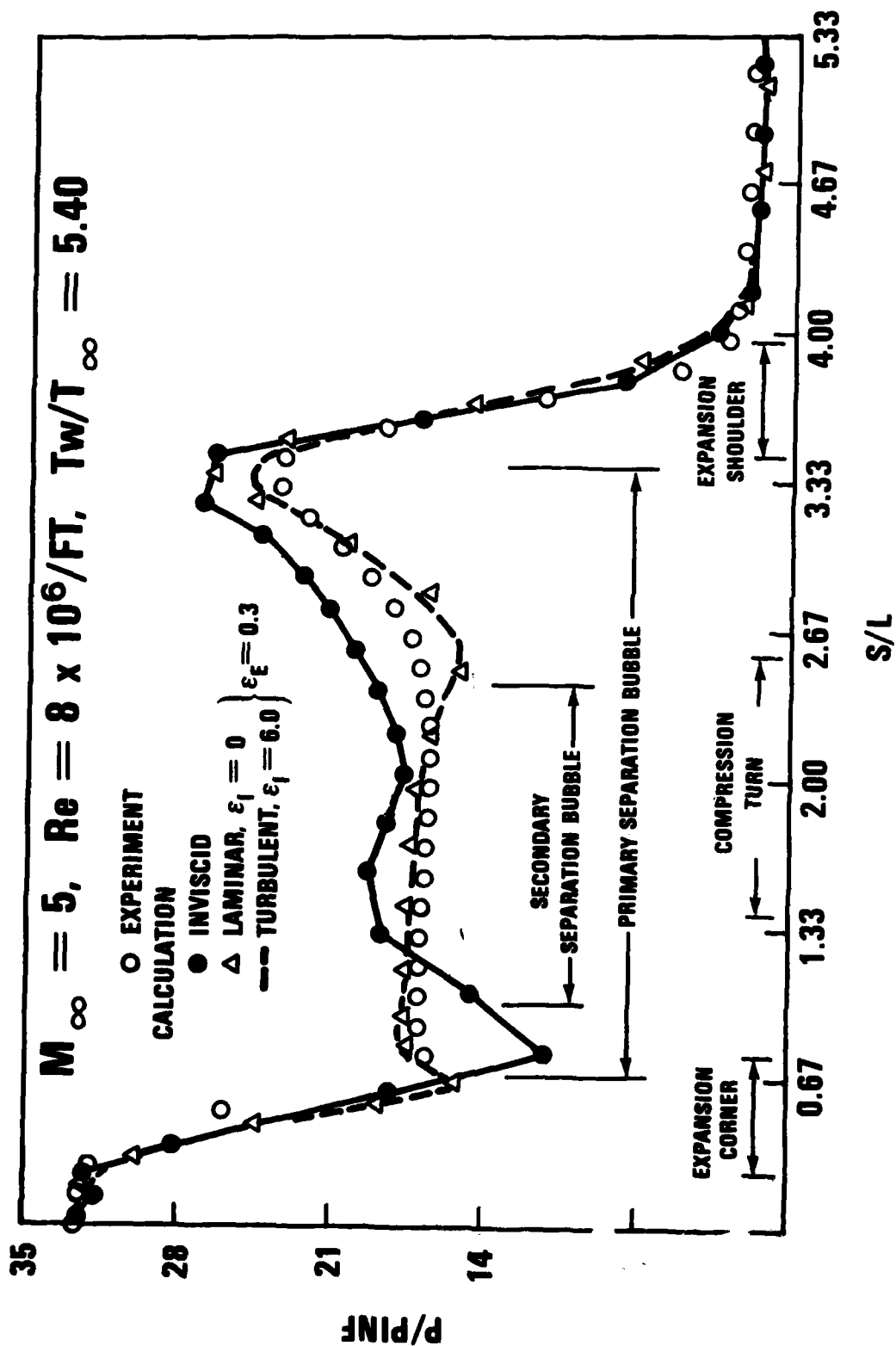Figure 3   Comparison of Shock Location Between Calculation and Experiment for Model 4

Figure 4   Comparison of Surface Pressure Between Calculation and Experiment for Model 4
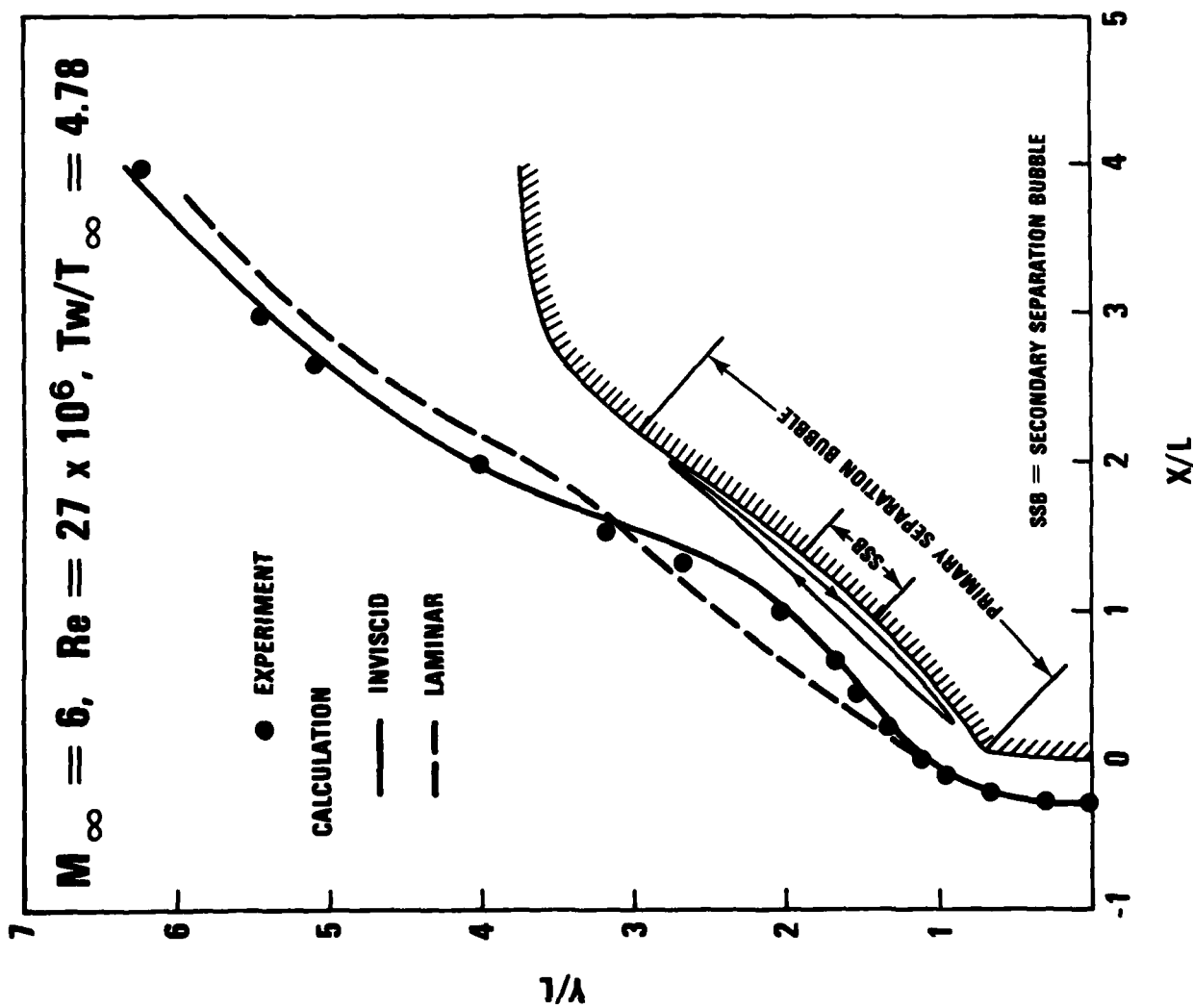
Figure 5   Comparison of Shock Location Between Calculation and
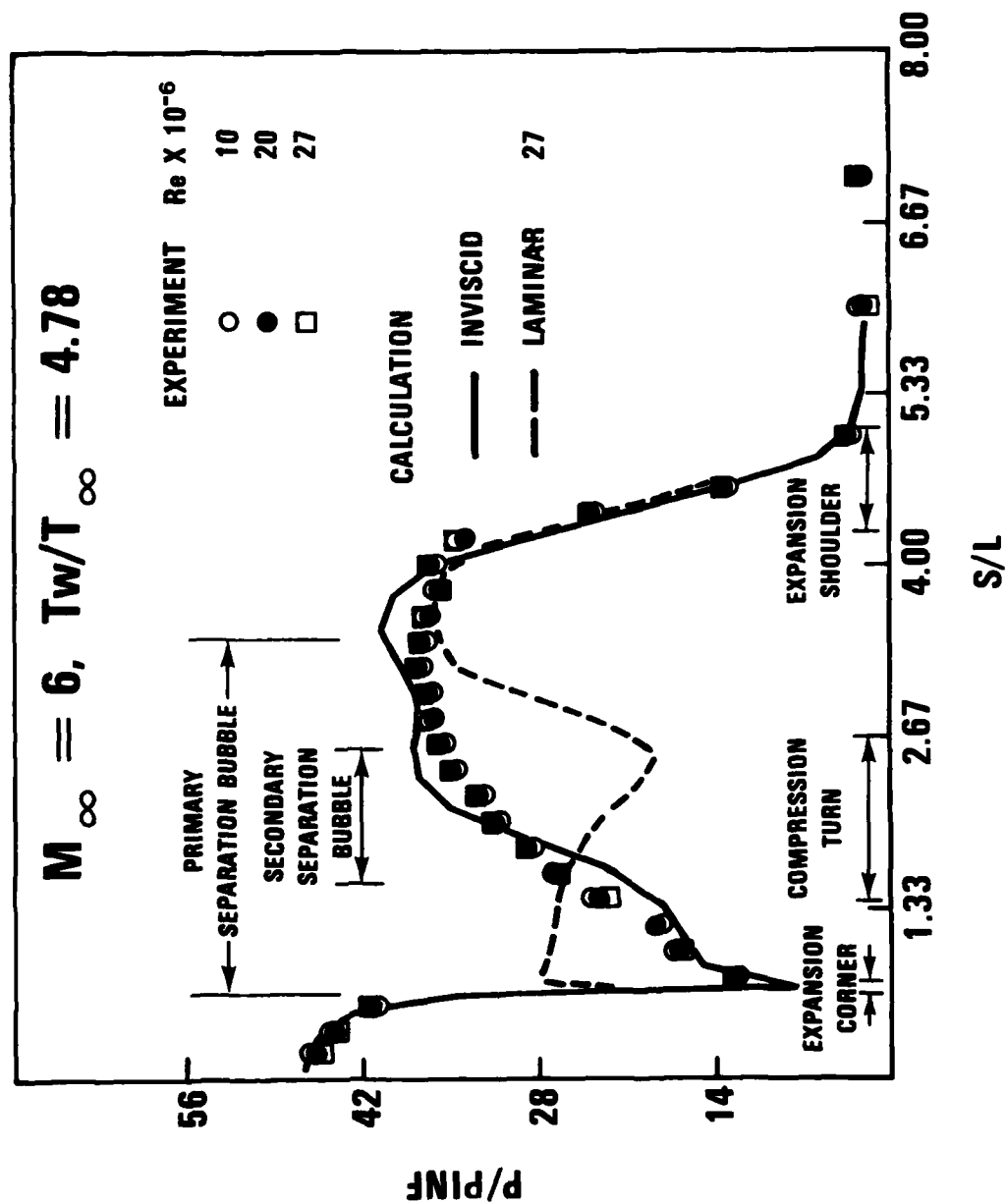Experiment for Model 1

Figure 6   Comparison of Surface Pressure Between Calculation
            and Experiment for Model 1